Human retinal gene therapy for Leber congenital amaurosis shows advancing retinal degeneration despite enduring visual improvement

Artur V. Cideciyan[a,1], Samuel G. Jacobson[a], William A. Beltran[b], Alexander Sumaroka[a], Malgorzata Swider[a], Simone Iwabe[b], Alejandro J. Roman[a], Melani B. Olivares[a], Sharon B. Schwartz[a], András M. Komáromy[b,c], William W. Hauswirth[d], and Gustavo D. Aguirre[b]

[a]Scheie Eye Institute, Department of Ophthalmology, University of Pennsylvania Perelman School of Medicine, Philadelphia, PA 19104; [b]Section of Ophthalmology, School of Veterinary Medicine, University of Pennsylvania, Philadelphia, PA 19104; [c]Small Animal Clinical Sciences/Veterinary Medicine, Michigan State University, East Lansing, MI 48824; and [d]Department of Ophthalmology, University of Florida, Gainesville, FL 32610

Edited by Jeremy Nathans, Johns Hopkins University, Baltimore, MD, and approved December 19, 2012 (received for review November 1, 2012)

Leber congenital amaurosis (LCA) associated with retinal pigment epithelium-specific protein 65 kDa (*RPE65*) mutations is a severe hereditary blindness resulting from both dysfunction and degeneration of photoreceptors. Clinical trials with gene augmentation therapy have shown partial reversal of the dysfunction, but the effects on the degeneration are not known. We evaluated the consequences of gene therapy on retinal degeneration in patients with *RPE65*-LCA and its canine model. In untreated *RPE65*-LCA patients, there was dysfunction and degeneration of photoreceptors, even at the earliest ages. Examined serially over years, the outer photoreceptor nuclear layer showed progressive thinning. Treated *RPE65*-LCA showed substantial visual improvement in the short term and no detectable decline from this new level over the long term. However, retinal degeneration continued to progress unabated. In *RPE65*-mutant dogs, the first one-quarter of their lifespan showed only dysfunction, and there was normal outer photoreceptor nuclear layer thickness retina-wide. Dogs treated during the earlier dysfunction-only stage showed improved visual function and dramatic protection of treated photoreceptors from degeneration when measured 5–11 y later. Dogs treated later during the combined dysfunction and degeneration stage also showed visual function improvement, but photoreceptor loss continued unabated, the same as in human *RPE65*-LCA. The results suggest that, in RPE65 disease treatment, protection from visual function deterioration cannot be assumed to imply protection from degeneration. The effects of gene augmentation therapy are complex and suggest a need for a combinatorial strategy in *RPE65*-LCA to not only improve function in the short term but also slow retinal degeneration in the long term.

neurodegeneration | outer nuclear layer | retinal structure

Hereditary blindness can be caused by genetic defects in retinal pigment epithelium (RPE) cells, where a continuous supply of 11-*cis*-retinal chromophore is produced by the visual cycle, or in photoreceptors, where light photons captured by chromophore molecules signal vision (1). One of the key components of the visual cycle is the retinoid isomerase encoded by the RPE-specific protein 65 kDa (*RPE65*) gene (2). Mutations in *RPE65* cause Leber congenital amaurosis (LCA), a severe childhood blindness (3). *RPE65*-associated LCA (*RPE65*-LCA) is a complex disease in which vision loss results from two pathological mechanisms—dysfunction and degeneration of photoreceptors (3–6). *RPE65*-LCA has been proclaimed to be the first successfully treated inherited retinopathy using gene augmentation therapy (7–10), and the treatment has resulted in substantial improvement in vision that endures at least 3 y (11).

Whereas we showed that gene therapy corrects the biochemical blockade leading to visual dysfunction and converts *RPE65*-LCA from a two-mechanism disease into a simple retinal degeneration (9), it has not been determined if therapy also treats the retinal degeneration component. It is hypothesized that correction of the underlying cellular dysfunction in a human recessive retinal degeneration will promote greater neuronal survival by slowing the natural rate of photoreceptor loss. Gene therapy experiments that have evaluated photoreceptor degeneration have been performed mainly in mouse and dog models treated at young ages (12–18) and have implied that at least a subset of photoreceptors could be rescued from degeneration. However, accumulating evidence has suggested that human *RPE65*-LCA, which can show degeneration prenatally or within the first years of life (19, 20), is better modeled at the more advanced disease stages in older animals (3, 21).

We evaluated the visual function and retinal degeneration in treated and untreated eyes of patients with *RPE65*-LCA and in the dog model of this disease. Gene therapy resulted in remarkable and lasting improvements in visual function, but serial measurements of outer photoreceptor nuclear layer (ONL) thickness showed continuing progression of photoreceptor loss. Our human and canine results are consistent with the hypothesis that the majority of photoreceptors in the degenerative phase of *RPE65* disease is destined for progressive loss. Treatment of *RPE65*-LCA should evolve into a two-pronged intervention that not only leads to visual restoration in the short term but also, improved photoreceptor survival in the long term.

Significance

The first retinal gene therapy in human blindness from *RPE65* mutations has focused on safety and efficacy, as defined by improved vision. The disease component not studied, however, has been the fate of photoreceptors in this progressive retinal degeneration. We show that gene therapy improves vision for at least 3 y, but photoreceptor degeneration progresses unabated in humans. In the canine model, the same result occurs when treatment is at the disease stage equivalent to humans. The study shows the need for combinatorial therapy to improve vision in the short term but also slow retinal degeneration in the long term.

Author contributions: A.V.C., S.G.J., W.A.B., A.M.K., W.W.H., and G.D.A. designed research; A.V.C., S.G.J., W.A.B., A.S., M.S., S.I., A.J.R., M.B.O., S.B.S., A.M.K., W.W.H., and G.D.A. performed research; A.S., M.S., and A.J.R. contributed new reagents/analytic tools; A.V.C., S.G.J., W.A.B., A.S., M.S., A.J.R., M.B.O., S.B.S., W.W.H., and G.D.A. analyzed data; and A.V.C., S.G.J., W.A.B., W.W.H., and G.D.A. wrote the paper.

Conflict of interest statement: W.W.H. and the University of Florida have a financial interest in the use of adeno-associated virus therapies and own equity in a company (AGTC Inc.) that might, in the future, commercialize some aspects of this work. The remaining authors declare no conflict of interest. University of Pennsylvania, University of Florida, and Cornell University hold a patent on the described gene therapy technology (United States Patent 20070077228, "Method for Treating or Retarding the Development of Blindness").

This article is a PNAS Direct Submission.

[1]To whom correspondence should be addressed. E-mail: cideciya@mail.med.upenn.edu.

This article contains supporting information online at www.pnas.org/lookup/suppl/doi:10.1073/pnas.1218933110/-/DCSupplemental.

Results

Human *RPE65*-LCA: Natural History of Photoreceptor Degeneration. Our cohort of *RPE65*-LCA patients (Tables S1 and S2), including those patients as young as 3 y of age, had abnormal ONL thickness at a majority of sampled retinal locations (Fig. S1), consistent with previous reports of loss of photoreceptors detectable at the earliest ages evaluated to date (6, 19, 20, 22–24). Untreated *RPE65*-LCA eyes were examined longitudinally to measure the rate of progression of this early-onset retinal degeneration. Patient 23 (P23) illustrates the spatiotemporal progression of retinal degeneration (Fig. 1 *A*–*D*). Optical coherence tomography (OCT) scans across a 15-mm extent along the vertical meridian crossing the fovea (Fig. 1*A*) show the intraretinal backscattering differences that delineate retinal sublaminae corresponding to different cell layers (20). Quantitatively, the ONL thickness shows changes at most retinal locations (Fig. 1 *A* and *B*). Thinning of the ONL fraction (ONL thickness of the patient divided by mean normal thickness at the same retinal location) at most extrafoveal retinal locations showed log-linear progression (Fig. 1*C*), which is consistent with a model wherein the photoreceptor degeneration follows an exponential decay after a retinal locus-specific onset of photoreceptor degeneration (25, 26). To a first approximation, kinetics of ONL loss followed similar exponential decay rates irrespective of retinal location. This invariant exponential decay was estimated from the median value of the population of slopes calculated from each of the consecutive pairs of measurements. The onset of progressive degeneration phase was estimated at each retinal location by extrapolating along the median slope to 0 log ONL fraction, and all of the data was replotted to illustrate how a single underlying natural history can predict disease progression across multiple retinal locations at different disease stages (Fig. 1*D*).

Fifteen patients (ages 7–29 y at first visit) (Table S1) were examined serially (over periods ranging from 1.2 to 6.7 y, average = 4.6 y) to understand better the inter- and intraretinal variation of the natural history of retinal degeneration in *RPE65*-LCA (Fig. 1*E*). ONL thickness fraction from all retinal locations and all patients showed a wide variation when plotted against chronological age (Fig. 1*E*). There was a weak negative correlation with age both at inferior (slope = −0.015 log/y; r^2 = 0.12) and superior (slope = −0.016 log/y; r^2 = 0.11) retinal loci (Fig. 1*E*). To form a predictive natural history of disease applicable to *RPE65*-LCA, we calculated the median of the exponential rates across all patients, all retinal locations, and all consecutive pairs of measures (n = 426). On adjustment for the individual and locus-specific onset of the progressive degeneration phase, the underlying natural history (Fig. 1*F*) was highly consistent (r^2 = 0.91) with a steeper slope (−0.04 $\log_{10}$/y) compared with the same data plotted against chronological age.

Natural History of Visual Sensitivity in Human *RPE65*-LCA. Patients with *RPE65*-LCA show a substantial loss of light sensitivity unexplained by the amount of underlying photoreceptors (3, 6, 10, 22, 27). It is important to emphasize, however, that the patients do not lose all visual function. Often, there is measurable remnant vision that is mediated by rods, cones, or both (11, 22, 27). The source of this remnant vision or its natural history is not understood in *RPE65*-LCA. We next asked the question: what would be the expected change in sensitivity during the time span of measured ONL thinning? For simple retinal degenerations, a change in sensitivity should be proportional to the square of the change in ONL thickness (6). For the median exponential degeneration rate of −0.04 log/y, the corresponding change in sensitivity would be −0.08 log/y (Fig. 1*G*, expected). Progression of vision loss is expected to be similar to simple retinal degenerations, although the absolute sensitivity is dissociated from ONL thickness (6). To evaluate this hypothesis, we measured the change in light sensitivity along the vertical meridian at the same retinal locations and in the same patients as those patients included for the study of ONL change over time (Table S1). Unexpectedly, there was little detectable change measured in sensitivity. A regression line fit to the visual function data over a time horizon extending to 6 y showed a slope of −0.02 log/y (Fig. 1*G*, observed; −0.007 log/y if the regression line was forced to go through the origin), which was more shallow than the slope expected from the underlying photoreceptor degeneration.

Gene Therapy Does Not Slow the Progressive Retinal Degeneration in *RPE65*-LCA. To determine the consequences of subretinal gene therapy on retinal degeneration, three analyses were performed: (*i*) intraocular comparisons were made of ONL fractions between treated and untreated retinal regions of the same eye; (*ii*) interocular comparisons were made of ONL fractions between study eyes and contralateral control eyes; and (*iii*) the progression of the ONL fraction in study eyes was compared with the expected natural history of *RPE65*-LCA. All analyses were performed along the vertical meridian. Treated regions in study eyes received the subretinal therapeutic vector and showed a significant improvement in visual function during the 90-d period after surgery. Control regions in study eyes did not receive the subretinal therapeutic vector and did not show change in visual function parameters during the same time period.

The first analysis is illustrated by the intraocular comparison data from the study eyes of P7 and P2; control [Fig. 2*A*, red bars (inferior retina)] and treated [Fig. 2*A*, green bars (superior retina)] regions are shown. For the control region in P7, the mean ONL fraction was 0.73 at baseline and reduced to 0.45 at 3 y later. For the treated region, the ONL fractions were 0.52 and 0.32 at baseline and 3 y later, respectively. Results in the study eye of P2 showed a similar reduction of ONL fraction at 3 y compared with baseline for both types of regions (from 0.57 to 0.38 at the control region and from 0.49 to 0.35 at the treated region). When ONL fractions from study eyes were compared, there was no significant difference (P = 0.91, Mann–Whitney rank sum) at baseline between regions (treated quartiles = 0.22, 0.40, 0.57; untreated quartiles = 0.24, 0.29, 0.57). At the last available visit after the treatment (Table S2), retinal regions showed thinner ONL compared with baseline, but there remained no significant difference (P = 0.66) between treated and untreated regions (treated quartiles = 0.17, 0.25, 0.36; untreated quartiles = 0.16, 0.26, 0.42).

In the second analysis, ONL fractions from treated study eyes and untreated control eyes (Tables S1 and S2) were compared. There was no significant difference (P = 0.70, Mann–Whitney rank sum) at baseline between eyes (study eye quartiles = 0.22, 0.40, 0.57; control eye quartiles = 0.22, 0.33, 0.51) when considering matched retinal regions (n = 36 regions in nine patients) that were later found to have been successfully treated in study eyes. At the last available visit, retinal regions showed thinner ONL compared with baseline, but there remained no significant difference (P = 0.99) between the eyes (study eye quartiles = 0.17, 0.25, 0.36; control eye quartiles = 0.16, 0.26, 0.44). Similarly, for untreated regions in study eyes and their matched regions in control eyes (n = 37 regions in nine patients), there were no significant differences in ONL fraction at baseline (P = 0.79) or at the last visit (P = 0.52).

In the third analysis, data from study eyes were compared with the expected model of the natural history of degeneration (Fig. 2*B*). For these analyses, the start of the degeneration phase was estimated from the ONL thickness fraction measured at baseline, and all posttreatment time points were then plotted with respect to the baseline value. The great majority of 45 control regions (11 eyes) (Fig. 2*B*, *Left*) showed progressive thinning of the ONL that was not substantially different from the natural history observed in untreated eyes. There were rare locations that showed no change or greater than expected deviation. For the 36 treated regions, the results were similar (nine eyes) (Fig. 2*B*, *Right*); the

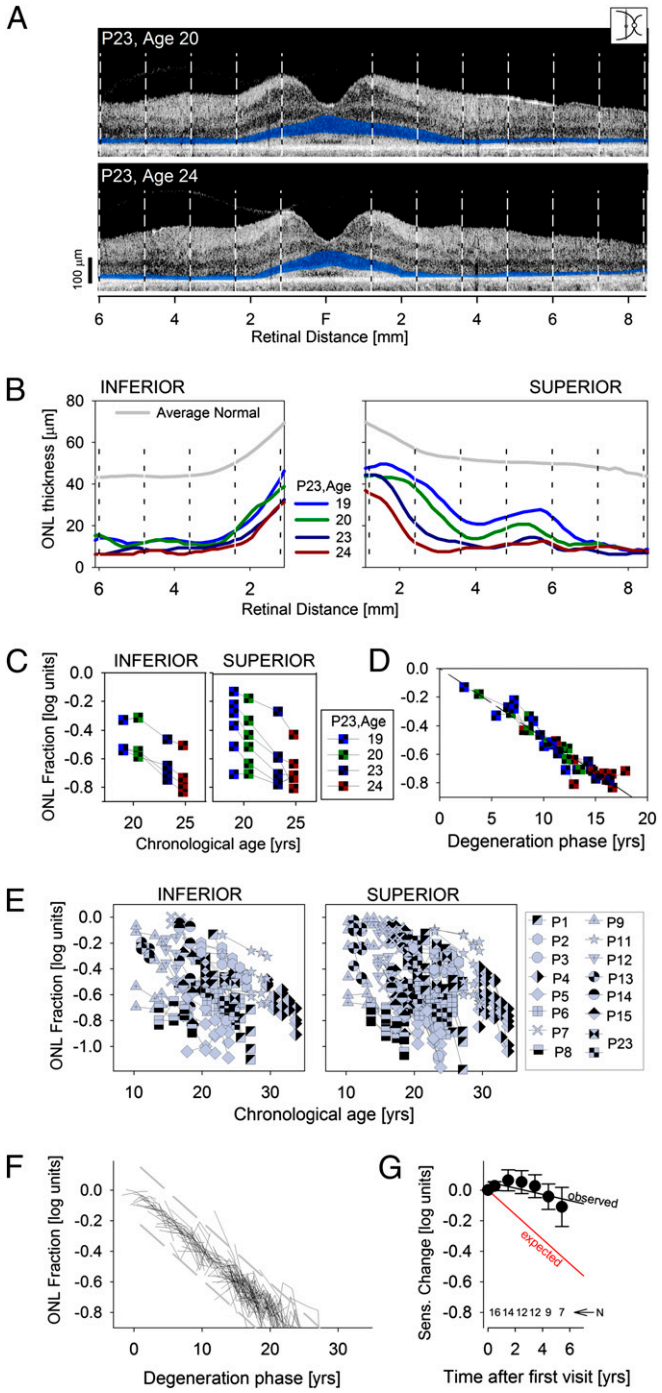

Fig. 1. Natural history of disease in untreated human *RPE65*-LCA. (*A*) Cross-sectional OCT retinal scans in P23 performed along the vertical meridian (*Inset*) at ages 20 and 24 y. Vertical dashed lines delimit the 10 extrafoveal regions quantified. ONL is highlighted in blue for visibility. F, fovea. (*B*) ONL thickness of P23 as a function of eccentricity at ages 19, 20, 23, and 24 y shows progressive thinning at most retinal locations. (*C*) Logarithm of the ONL fraction against age supports an underlying exponential decay function describing progression. (*D*) Data from *C* replotted after horizontal shifts accounting for differences in the onset of degeneration at each retinal region. (*E*) ONL thickness in untreated *RPE65*-LCA eyes shows an extremely wide spectrum of results with a weak tendency of thinning as a function of chronological age. (*F*) Data from *E* replotted after horizontal shifts accounting for differences in age of onset. Results show a predictable natural history underlying the progressive degeneration in most patients. Dashed lines delimit the range of deviation (±2 SD) of the data from the model. (*G*) Average visual sensitivities measured at the same retinal locations in the same patients are stable over time and do not conform to the expected slope (red) estimated from the ONL degeneration. Error bars are SE. Numbers of eyes contributing to each data point are shown.

great majority progressed along the expected natural history, with rare regions showing no change or greater than expected deviation. When the ONL fraction deviations between the measured data and the natural history model were compared, there were no statistically significant differences between treated regions in study eyes, control regions in study eyes, and all loci in untreated eyes ($P = 0.81$, Kruskal–Wallis ANOVA on ranks). In summary, all three analysis methods supported the conclusion that gene therapy has not modified the natural history of progressive retinal degeneration in the *RPE65*-LCA patients.

Early Visual Improvements Persist Up to 3 y After Human Gene Therapy. Visual sensitivity at the control regions of treated eyes was not significantly changed compared with baseline (Fig. 2*C*). The regression line showed a nearly zero slope (0.02 log/y) instead of a slope of −0.08 log/y expected based on the retinal degeneration rate estimated at the same retinal locations. In a subset of patients, visual function data for up to 4.5 y (average = 2.1 y, $n = 6$) before treatment were available (Fig. 2*C*, purple symbols) and consistent with the stability observed posttreatment. These results mirrored our observations in untreated control eyes (Fig. 1*G*). At the treated retinal locations, there were substantial improvements in visual sensitivity averaging 1.6 (range = 0.8–2.4) log units better than baseline within a short (30–90 d) period (Fig. 2*C*). Long-term evaluation of the treated locations showed mostly stability or additional improvement of the sensitivities (Fig. 2*C*, regression slope 0.04 log/y), results that were in contrast to the continuing degeneration measured at the same locations of the same eyes (Fig. 2*B*).

Natural History of Photoreceptor Degeneration in *RPE65*-Mutant Dogs. Next, we asked whether the posttreatment results of advancing retinal degeneration despite enduring visual improvement were unique to human *RPE65*-LCA or also occurred in an animal model of the disease. *RPE65*-mutant dogs are the only large animal model for *RPE65*-LCA and are known to show congenital visual dysfunction followed later by retinal degeneration (5, 17, 28–32). First, we defined the natural history of the canine disease. The thickness of the ONL layer recorded with noninvasive cross-sectional OCT retinal imaging was used to estimate the spatial pattern of the onset and progression of the retinal degeneration. Histological data in a limited number of dogs were also used in the analyses. Normal dogs showed thicker ONL in the superior (tapetal; nonpigmented RPE) retina compared with inferior (nontapetal; pigmented RPE) retina (Fig. 3*A*). *RPE65*-mutant dogs at 5 y of age could show nearly normal ONL thickness topography (Fig. 3*B*). By 8 y of age, there was substantial thinning of the ONL, with detectable photoreceptors remaining across the central (visual streak) retina extending into the superior retina (Fig. 3*C*).

Five locations in inferior, superior, and central retina were chosen (squares in Fig. 3 *A*–*C*) to quantify the natural history of ONL changes in *RPE65*-mutant dogs compared with normal dogs (Table S3). At all five locations, normal eyes showed a small amount of ONL thinning (−0.014 log/y) over the first 8 y of dog life (Fig. 3 *D*–*F*, gray circles and lines). In *RPE65*-mutant eyes, at the two inferior retinal loci, ONL fraction measurements were consistent with the onset of the photoreceptor degeneration occurring near 4.9 y (Fig. 3*D*). At the two superior retinal loci, there was a similar natural history, but disease onset was delayed to 5.3 y (Fig. 3*E*). At the central retinal locus (nasal to the optic nerve on or near the visual streak), most of the eyes showed normal or near-normal ONL thickness. Limited data from a 10-y-old dog

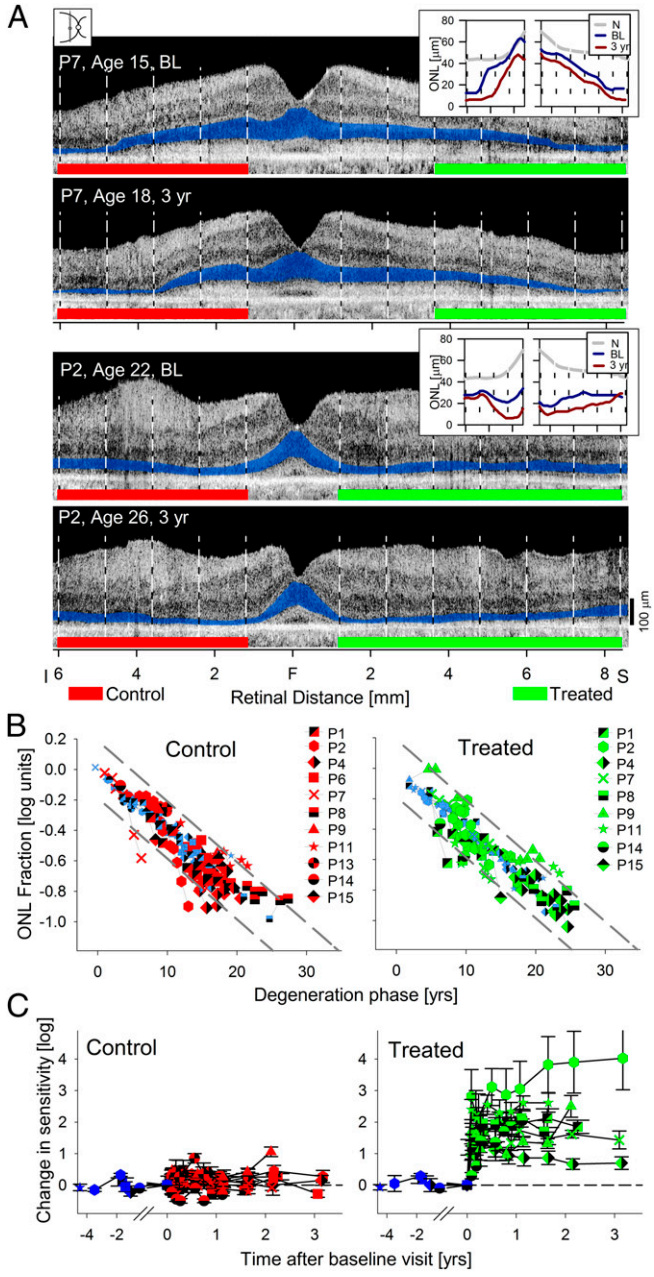

Fig. 2. Photoreceptor degeneration in human *RPE65*-LCA eyes that have had gene therapy. (*A*) Cross-sectional OCT scans in two patients, P7 and P2, at baseline (BL) and 3 y after treatment. Green lines demarcate the region superior to the fovea that received a subretinal injection and that visual function measurements showed significant improvements in sensitivity. Red lines demarcate the untreated control retinal regions. ONL is highlighted in blue for visibility. (*Insets*) Thickness of the ONL at BL and posttreatment time points compared with mean normal (N) shows degeneration occurring at most loci. (*B*) ONL measures in control (*Left*) and treated (*Right*) retinal regions plotted on the natural history of *RPE65*-LCA disease defined in Fig.1. The progression in control and treated regions is, for the most part, indistinguishable from the natural history. (*C*) Visual sensitivities measured at control (*Left*) and treated (*Right*) retinal locations in the same patients. Control locations show stable sensitivities before and after surgery. Treated locations show a dramatic improvement after the surgery that is retained over time. Pretreatment measures are shown with purple symbols in *B* and *C*.

were consistent with the onset of photoreceptor degeneration being delayed to as much as 7 or more y (Fig. 3*F*). In summary, *RPE65*-mutant dogs displayed only the dysfunction component of the RPE65 disease for an extended period ranging to at least one-quarter of their lifespan. Onset of retinal degeneration in *RPE65*-mutant dogs occurs relatively late at ages equivalent to ∼30 human y (33).

Gene Therapy in *RPE65*-Mutant Dogs Rescues Progressive Retinal Degeneration only When Delivered Before the Onset of Retinal Degeneration. Results from two dogs illustrate the long-term success in preventing the photoreceptor loss when *RPE65* gene therapy is delivered before the onset of retinal degeneration (Fig. 4 *A* and *B*). Dog 23 (D23) received a subretinal injection in the central and inferior nasal retina of the right eye at the age of 0.3 y. Electroretinogram (ERG) recordings for the first 3 y after treatment were markedly improved for rod and cone amplitudes compared with untreated eyes (34, 35). ERGs at age 9.7 y remained sizable, suggesting a durability of functional gains by rods and cones for nearly a decade (Fig. S2). By OCT, ONL thickness was undetectable outside the injected region, but there was substantial ONL remaining within the treated region (Fig. 4*A*). Quantitative results were consistent with nearly normal ONL thickness within the treated region in infero-nasal and central retina (Fig. 4 *C* and *E*, green diamonds), relatively retained ONL in the supero-nasal retina (Fig. 4*D*, green diamond), and severe retinal degeneration consistent with the natural history of disease in untreated supero-temporal and infero-temporal retinal locations (Fig. 4 *C* and *D*, red diamonds). D25 received, at age 1.9 y, a subretinal injection that extended from near the optic nerve into superior retina. ERG recording nearly 5 y after the treatment at 6.7 y showed significant functional improvement (Fig. S2). ONL thickness topography at age 6.7 y indicated that there was a retained area corresponding to the treatment region (Fig. 4*B*). Quantitative results in the inferior untreated retina were consistent with the natural history (Fig. 4*C*, red up triangles). In the treated superior retina, however, ONL thickness in D25 was within the normal range and substantially greater than expected from the natural history of RPE65 disease (Fig. 4*D*, green up triangles). The treated one-half of the central retinal region of D25 had near-normal ONL thickness, which was expected from the natural history. These results underscore the importance of understanding spatiotemporal distribution of the disease to interpret therapeutic effects (Fig. 4*E*).

ONL thickness mapping and quantitative measurements were performed in three additional eyes (D24, D26, and D27) (Table S3) injected subretinally in the superior retina at ages 1.8–2.4 y and evaluated at ages 6.6–7.2 y (Fig. 4 *C*–*E*). All three eyes showed significant ERG improvements nearly 5 y after the treatment at ages of ∼7 y (Fig. S2). ONL fraction in control regions outside of the injection region was not different from the natural history of *RPE65* disease in dogs (Fig. 4 *C* and *E*, smaller red symbols). In treated superior retinal regions, ONL fraction was normal or near normal, showing substantial rescue compared with the natural history of RPE65 disease (Fig. 4*D*, smaller green symbols).

The eyes of the five early-treated dogs were examined by histology at the end of the study (Table S3). Histology results were well-correlated with those results obtained with noninvasive OCT imaging. The findings for D23, D25, and D26 are illustrated (Fig. 5 and Fig. S3). In general, photoreceptor morphology was normal in the center of the treatment area, with an intact ONL and preservation of inner retinal layers (Fig. 5*B* and Fig. S3 *B* and *E*). Towards the margins of the treatment areas, the ONL gradually thinned, and photoreceptors became shorter, broader, and more disoriented (Fig. 5*C* and Fig. S3*C*). Outside the treatment boundary, there was an abrupt loss of photoreceptors, with prominent retinal gliosis and loss of layer organization (Fig. 5*D*). RPE65 immunolabeling showed distinct cytoplasmic labeling within the treatment areas (Fig. 5*B1*), but none outside (Fig. 5*D1*). It appeared that RPE65 expression was most intense in the center of the treatment area and less intense and uniform towards the edges.

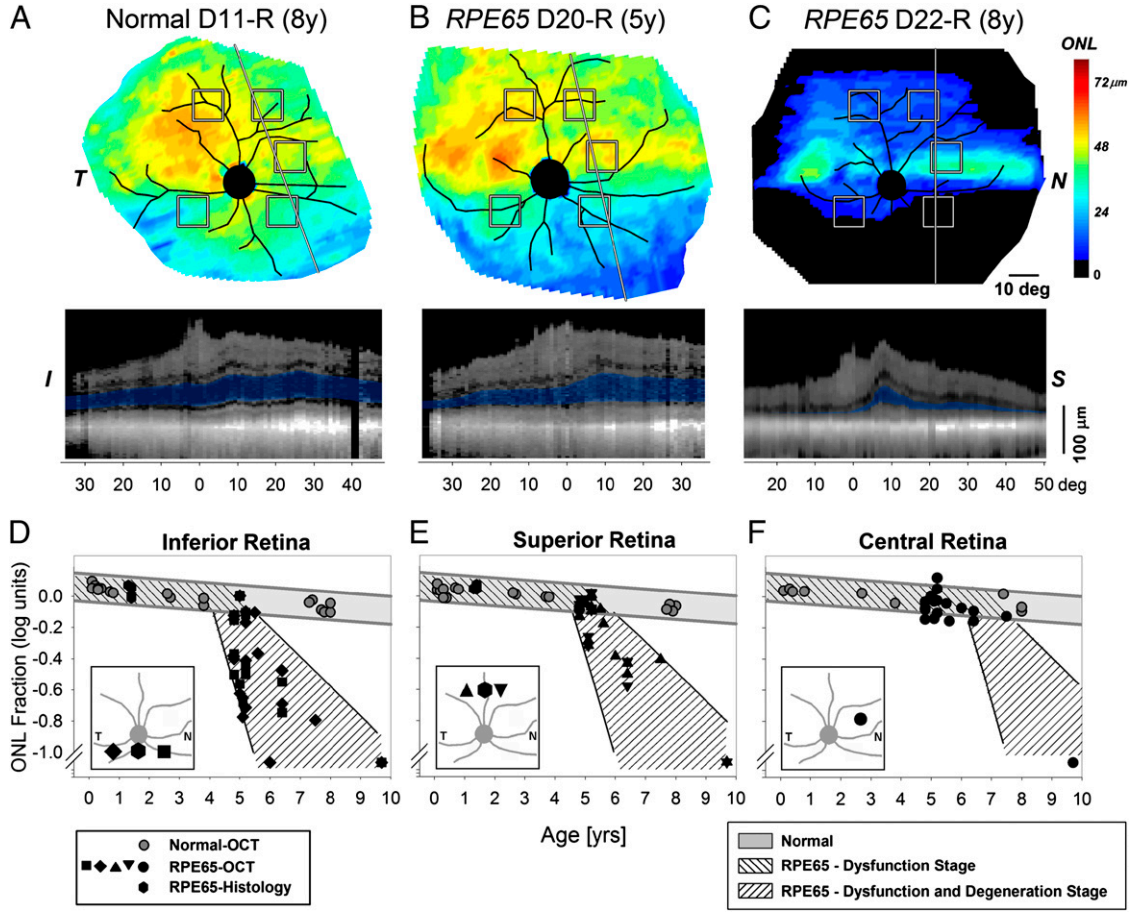

Fig. 3. Natural history of retinal degeneration in *Rpe65*-mutant dogs shows regional effects. (*A–C*) Photoreceptor (ONL) thickness topography in a normal dog compared with two *Rpe65*-mutant dogs at different ages. ONL thickness topography is mapped to a pseudocolor scale. *I*, inferior; *N*, nasal; *S*, superior retina; *T*, temporal. Reconstituted OCT scans along a superior–inferior meridian (line) are shown in *Lower* with the ONL layer highlighted in blue. Retinal distances are specified relative to the point closest to the optic nerve. Note that the OCTs shown are reconstituted from ultra-wide angle maps covering more than 80° × 80° (~24 × 24 mm) sampled at 1°. (*D–F*) ONL thickness quantified as a function of age at five retinal locations (shown as squares in *A–C*): two inferior loci (*D*), two superior loci (*E*), and a nasal central visual streak locus (*F*). Gray symbols represent normal animals; black symbols represent *RPE65*-mutant dogs. Gray lines approximate the expected range of normal results. Hashed regions within gray lines show the dysfunction-only stage, and hashed regions within black lines show the dysfunction and degeneration stage of RPE65 disease. *Insets* are 60° × 60° and show the five retinal locations sampled with OCT and two locations sampled with histology. Overlapping symbols have been moved horizontally to aid in their visibility.

Of interest, regardless of the expression of the RPE65 transgene in the treated regions, there were no apparent changes in the size and number of the vacuolated RPE inclusions that are characteristic of the disease (35).

When gene therapy was performed in eyes of mutant dogs older than 4.8 y (Table S3), an age when at least part of the retina shows photoreceptor loss in most of the animals, visual function improved within 1 mo (Fig. S2), but retinal structural results obtained 1 y later did not show a positive modification of the natural history of photoreceptor degeneration (Fig. 4 *F–J*). Illustrating these results are D19 injected in the infero-temporal retina (Fig. 4*F*) and D22 injected in the supero-nasal retina (Fig. 4*G*) at ages 5.1 and 6.4 y, respectively. When imaged more than 1 y later, there was no obvious retention of ONL thickness corresponding to the treated regions. Quantitative results in dogs treated after 4.8 y of age (D16, D17, D19, and D22) showed ONL fraction consistent with the expected natural history of disease both in treated (Fig. 4 *H–J*, green symbols) and untreated (Fig. 4 *H–J*, red symbols) locations. These results are consistent with the hypothesis that gene therapy after the onset of retinal degeneration did not substantially modify the natural history of disease in the mutant dog.

Discussion

Gene augmentation therapy for human *RPE65*-LCA, as performed in four independent clinical trials, has resulted in substantially improved visual function within days to weeks after treatment (7–10), and the functional gain has been durable for as long as 3 y (11, 36) (Fig. 2*C*). These positive results bode well for the ability of gene therapy to partially ameliorate the severe and lifelong visual impairment experienced in *RPE65*-LCA. It is important to remember, however, that this vision loss is caused by a combination of a biochemical chromophore deficiency and a progressive degeneration of cone and rod photoreceptor cells (3). Restoration of RPE65 expression through gene therapy is thought to treat the chromophore deficiency, but it has also been assumed that treating the primary biochemical deficiency would slow or arrest the (presumed) secondary degeneration. Here, we test this assumption by determining if there is progression of retinal degeneration in patients with *RPE65*-LCA treated with gene therapy. We find that gene therapy causes substantial and durable vision improvement but does not slow the natural history of photoreceptor degeneration. Our findings have similarities to treatments applied to the CNS that lessen symptoms but do not slow the neurodegeneration (37, 38). The practical implication

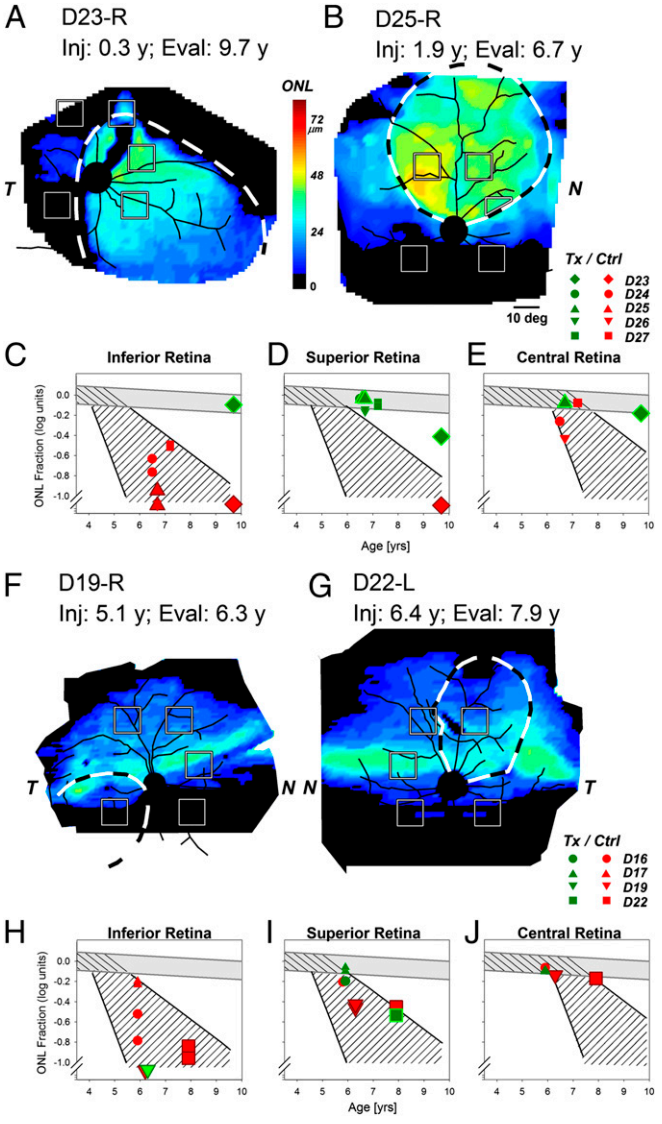

Fig. 4. Gene therapy applied before and after the onset of retinal degeneration in *Rpe65*-mutant dogs. (*A* and *B*) Photoreceptor (ONL) thickness topography in two dogs (D23 and D25) treated before the onset of the degeneration and evaluated ∼5–9 y later. There is much better retention of ONL thickness within the treatment region (dashed lines) compared with outside the treatment region. (*C–E*) ONL thickness quantified as a function of age at five retinal locations in five dogs treated before the initiation of degeneration. Red symbols correspond to retinal locations outside the treatment region, and green symbols correspond to locations within the treatment region. (*F* and *G*) ONL thickness topography in two dogs (D19 and D22) treated after the onset of degeneration. There is no evidence for thicker ONL within the treatment regions compared with outside the treatment regions. (*H–J*) ONL thickness quantified as a function of age at five retinal locations in treated eyes. Both untreated control (red symbols) and treated (green symbols) regions are not substantially different compared with the natural history of disease. Larger symbols in *C–E* correspond to data shown in *A* and *B*, and larger symbols in *H–J* correspond to data shown in *F* and *G*.

of our results is that human treatments of *RPE65*-LCA should address the need to slow or arrest the retinal degeneration that is present and ongoing in these patients, no matter how young they are when considered for enrollment in clinical trials to treat the dysfunction component of their complex disease.

To determine success of any treatment intended to slow the rate of retinal degeneration, an estimate should first be made of the rate of natural progression without treatment. For *RPE65*-LCA, the momentum toward treatment in the clinic was so great after proof-of-concept success in animals that there was no waiting for natural history data to emerge. Treatment for a genetic retinal disease, for the first time in history, took priority, and early reports of visual improvement seemed to validate that it was unnecessary to establish a rate of retinal degeneration. Now, as plans are announced to extend these initial trials to treating very young patients, both eyes, and greater retinal areas, we felt the need to revisit first principles. We made serial measurements of ONL thickness in untreated eyes of *RPE65*-LCA patients and estimated the rate of photoreceptor loss to be, on average, −0.04 $\log_{10}$/y (−9.6%/y) under a delayed exponential model of disease (25, 39–41). This progression rate is comparable with the rate estimated in a different retinal degeneration caused by *MYO7A* mutations using similar methods and longitudinal data (26) and within the range of progression rates estimated from visual function measures in other retinal degenerative diseases (25, 40, 41).

How do our estimates of the rate of progression of retinal degeneration in human patients compare with animal models of *RPE65*-LCA? *Rpe65*$^{-/-}$ mice show an onset of degeneration near 3–4 mo (4, 42) and a degeneration rate averaging −0.22 $\log_{10}$/y (21). Assuming an allometric relationship between rates of neurodegeneration and maximum lifespan (33), the *Rpe65*$^{-/-}$ mouse disease is much slower than human disease (6, 19–24, 43–45), with an onset that is equivalent to 9–12 human y and a rate that corresponds to −0.006 $\log_{10}$/human y. *RPE65*-mutant dogs were also known to have slow photoreceptor degeneration (5, 29, 30, 32), but the details of spatiotemporal progression were unknown. Our results showed that the onset of degeneration ranges from 5 to 8 y depending on retinal location. By allometric scaling, this range corresponds to 31–48 human y. The progression rate in *RPE65*-mutant dogs averaged −0.33 $\log_{10}$/y, corresponding to −0.05 $\log_{10}$/human y. Thus, both murine and canine models show an extended period (up to 25% of their lifespan) with a retina-wide dysfunction-only phase that does not seem to have an equivalent in human *RPE65*-LCA at any age observed to date (6, 19–24, 43–45). Human *RPE65*-LCA is best modeled in older animals clearly displaying the dysfunction as well as degeneration phases of RPE65 disease. During this combined phase, the rate of progression in the canine model seems to be more similar to the human disease compared with the rate observed in the murine model.

Preclinical experiments of gene augmentation therapy have been mostly performed in young *RPE65*-mutant animals at a disease stage preceding the onset of photoreceptor degeneration, and most investigations have focused on the restoration of visual function and safety of the intervention (12, 13, 34, 35, 46–52). Here, we evaluated the retinal degeneration in five younger dogs treated during the dysfunction-only stage of disease by longitudinally following them for 5–11 y after treatment. The results showed unequivocal survival of the photoreceptors within the treated region that would have otherwise degenerated. Noninvasive OCT studies localized the region of preservation, and histological studies showed intact ONL and preservation of inner retinal layers. Our studies confirm and extend previous studies (14, 17, 35), and they support the hypothesis that, in *RPE65*-mutant dogs, early treatment of the primary RPE defect prevents the later onset of photoreceptor degeneration. Similar experiments in mutant mice treated early with gene therapy have shown survival of cone (12, 13, 15, 16) and rod photoreceptors (49). Investigation of the mechanism(s) causing photoreceptor cell loss (18, 53–56) has been mostly performed in untreated eyes to date. Extension of such studies to eyes undergoing gene therapy (18) would be important to clarify molecular underpinnings of the observed modification of natural history. Furthermore, the newly discovered vitamin A isomerization pathway originating in Muller

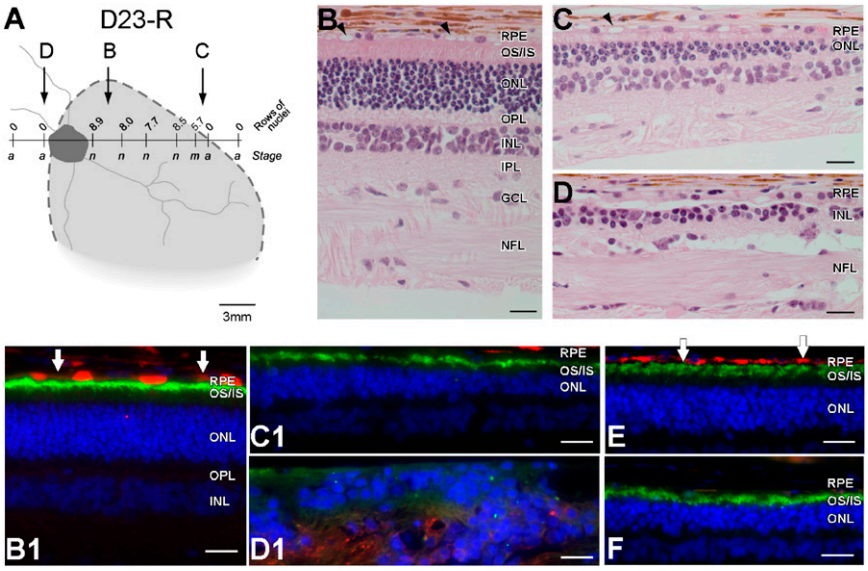

Fig. 5. Histologic evaluation of the *RPE65*-mutant dog D23 treated at 0.3 y before the onset of retinal degeneration shows remarkable rescue of photoreceptors from degeneration when assessed over a decade later. (*A*) Schematic representation of the *en face* image showing the treatment area (dashed lines), on which is superimposed the ONL rows (mean of three values in area sampled) and disease staging (*a*, advanced atrophy with gliosis and loss of retinal layer organization; *m*, moderate photoreceptor loss with 1/3 to 1/2 of ONL remaining; *n*, normal) assessed at 11.2 y. (*B–D*) Representative photomicrographs taken from areas identified in *A*. In the treatment area, there is normal retinal preservation (*B*), although the RPE shows vacuolated inclusions typical of the disease (arrowheads). At the edge of the treatment border (*C*), the photoreceptor layer becomes markedly attenuated and is absent (*D*) outside of the treatment region. (*B1*, *C1*, and *D1*) Double immunolabeling with RPE65 (red) and rod opsin (green) taken from regions corresponding to *B–D*. Labeling in RPE is present inside the treatment region (*B*), with some cells intensely labeled and others (vertical arrows) showing weaker immunolabeling. In the transition zone (*C1*), RPE65 labeling is absent, and opsin labeling reflects rod OS shortening and disorientation; outside the treatment area (*D1*), the photoreceptor layer is absent, and the inner nuclear layer (INL) is disorganized. (*E* and *F*) Control sections from WT dog (*E*) and *RPE65*-mutant dog in early stages of degeneration (*F*) show, respectively, the presence (red) or absence of specific RPE65 immunolabeling in the RPE. GCL, ganglion cell layer; NFL, nerve fiber layer; OPL, outer plexiform layer; OS/IS, outer and inner segment layer; INL, inner nuclear layer; IPL, inner plexiform layer. (Calibration: 20 μm.)

cells and subserving cones (57) may be found to contribute to the differences in (cone or rod) photoreceptor survival.

Our cohorts of *RPE65*-LCA patients who received gene therapy (9, 11, 36) showed remarkable and lasting improvements in visual function, but our serial measurements of ONL thickness now show that photoreceptor loss has continued along a trajectory no different from the expected natural history. In parallel experiments that we performed in older *RPE65*-mutant dogs, gene therapy applied after the onset of retinal degeneration did not seem to increase photoreceptor survival. To explain both findings, we postulate that there exists a critical limit in terms of accumulating molecular changes that are detrimental to photoreceptor survival under this condition of severe RPE65 dysfunction. There is evidence for molecular changes occurring in rod and cone photoreceptors in the predegenerative phase of RPE65 disease (17, 18, 32, 54, 58), and a specific translocation of one of the proapoptotic Bax isoforms from the cytosol to mitochondria has been observed to correlate with the initiation of photoreceptor cell loss (54, 55). To date, there has been a paucity of murine studies of gene therapy in older animals after the onset of retina-wide rod degeneration (6, 59). Expansion of such studies is required to better understand the molecular changes that are associated with inevitable loss of photoreceptors or successful protection from degeneration following gene augmentation therapy.

RPE65-mutant animals are not alone in requiring gene augmentation therapies to be applied in a predegenerative phase. Several murine models of primary photoreceptor diseases—such as mice with *Aipl1*, *Rpgrip1*, *Pde6b*, *Bbs4*, and *Cngb1* defects—show improved photoreceptor survival when therapies were applied before or at the early stages of retinal degeneration (60–64). To date, there has been only one demonstration of gene augmentation therapy applied after the onset of retinal degeneration that showed improved survival of photoreceptors (65). It remains to be determined whether this difference in outcome of canine retinitis pigmentosa GTPase regulator (RPGR) disease vs. other photoreceptor or RPE diseases in mouse models is because of species differences in the pathophysiology of disease or other treatment variables.

Untreated eyes of *RPE65*-LCA patients showed abnormal but stable visual function at the same retinal locations that were showing progressive loss of photoreceptors over the same observation period. Similarly, in treated eyes, the improved visual function in the short term did not diminish in the longer term with the progression of degeneration. These pairs of seemingly paradoxical findings may be explained by a number of hypotheses alone or combined. Two of these hypotheses involve the source of the remnant function driven by a chromophore, the identity, source, and concentration of which are currently unknown. A first hypothesis proposes that in *RPE65*-LCA, unliganded opsin molecules are in excess to chromophore molecules. Then the available chromophore would effectively limit detection of light, and visual function would be lost only when degeneration reduces the number of opsin molecules to be equal or less than the chromophore molecules available. A second hypothesis is that the chromophore production increases with progression of RPE65 disease and associated accumulation of retinyl esters within the RPE. This hypothesis has been raised to explain an age-related increase in sensitivity observed in *Rpe65*$^{-/-}$ mice (21). An increase in chromophore production could partially compensate for the loss of photoreceptors by increasing the proportion of regenerated opsin molecules in remaining cells. A third hypothesis would involve cones as the basis of stable visual function and the majority of rods showing the progressive degeneration. All three of these hypotheses could possibly explain the results in untreated eyes with ~5 log units loss of light sensitivity but are unlikely to explain the observations in the treated eyes, where (rod-mediated) sensitivities can

approach within 1 log unit of normal. A fourth hypothesis, more consistent with our data, is that *RPE65*-LCA photoreceptors show a spectrum of preapoptotic cellular stress states. At one end of the spectrum are functionally silent cells that are next in line to be lost to degeneration, and at the other end are healthier and functionally potent cells that will survive the longest. In this case, degeneration would progress with a constant rate of exponential decay after the disease onset (25, 26, 39–41). Initially, there would be little loss of function, but later, vision would be affected more and more at the late-disease stages with RPE atrophy, when there is loss of a critical number of last-remaining functionally potent (rod and cone) photoreceptors. Preliminary evidence for such a progression is observed as falling off a "cliff" of visual function near the peripheral boundaries of the visual field (27).

Gene augmentation therapy in *RPE65*-mutant patients, mice, and dogs has shown relative safety and remarkable improvement in visual function (11, 16, 35). Future human studies are being proposed to continue and expand the same therapeutic strategy. However, there is mounting evidence for a need to refine the initial approaches. One need for refinement is to understand sufficiently the visual cycle of human foveal cones to make the treatment efficacious for visual acuity (11). Another need, revealed in the present study, would be to seek a more complete therapeutic outcome that involves both visual improvement and structural rescue in extrafoveal retinal regions. The latter direction can be determined experimentally in older *Rpe65*-mutant mice and dogs that show both dysfunction and degeneration phases of the disease. In other words, there is a need to advance the therapy by taking a step back to proof-of-concept studies in animals at ages that better model the human patients. Among the possibilities to consider for refinement is delivery of agents to prevent the loss of retinal cells, such as neuroprotective, prosurvival, or antiapoptotic factors or antioxidants (66–69), sequentially or simultaneously with a more advanced version of gene augmentation therapy to increase chromophore to the remaining rod, extrafoveal cone, and foveal cone photoreceptors.

Materials and Methods

Human Subjects. Patients (n = 23) with *RPE65*-LCA were included (Tables S1 and S2). Informed consent was obtained. Procedures followed the Declaration of Helsinki guidelines and were approved by the institutional review board. Fifteen of the patients were enrolled in the clinical trial (NCT00481546). Methodological details are provided in *SI Materials and Methods*.

Dogs. *RPE65*-mutant (n = 16) and normal (n = 11) dogs were included (Table S3). All procedures involving animals (34, 35, 48, 65, 70) were performed in compliance with the Association for Research in Vision and Ophthalmology Statement for the Use of Animals in Ophthalmic and Vision Research and had Institutional Animal Care and Use Committee approval. Methodological details are provided in *SI Materials and Methods*.

ACKNOWLEDGMENTS. The clinical trial was supported by National Eye Institute Grant U10 EY 017280. Experimental work with the canine disease was funded by National Eye Institute Grants EY 06855, 017549, 019304, and 022012, and the Foundation Fighting Blindness.

1. Bramall AN, Wright AF, Jacobson SG, McInnes RR (2010) The genomic, biochemical, and cellular responses of the retina in inherited photoreceptor degenerations and prospects for the treatment of these disorders. *Annu Rev Neurosci* 33:441–472.
2. Palczewski K (2012) Chemistry and biology of vision. *J Biol Chem* 287(3):1612–1619.
3. Cideciyan AV (2010) Leber congenital amaurosis due to *RPE65* mutations and its treatment with gene therapy. *Prog Retin Eye Res* 29(5):398–427.
4. Redmond TM, et al. (1998) *Rpe65* is necessary for production of 11-*cis*-vitamin A in the retinal visual cycle. *Nat Genet* 20(4):344–351.
5. Aguirre GD, et al. (1998) Congenital stationary night blindness in the dog: Common mutation in the RPE65 gene indicates founder effect. *Mol Vis* 4:23.
6. Jacobson SG, et al. (2005) Identifying photoreceptors in blind eyes caused by *RPE65* mutations: Prerequisite for human gene therapy success. *Proc Natl Acad Sci USA* 102(17):6177–6182.
7. Bainbridge JW, et al. (2008) Effect of gene therapy on visual function in Leber's congenital amaurosis. *N Engl J Med* 358(21):2231–2239.
8. Maguire AM, et al. (2008) Safety and efficacy of gene transfer for Leber's congenital amaurosis. *N Engl J Med* 358(21):2240–2248.
9. Cideciyan AV, et al. (2008) Human gene therapy for RPE65 isomerase deficiency activates the retinoid cycle of vision but with slow rod kinetics. *Proc Natl Acad Sci USA* 105(39):15112–15117.
10. Banin E, et al. (2010) Molecular anthropology meets genetic medicine to treat blindness in the North African Jewish population: Human gene therapy initiated in Israel. *Hum Gene Ther* 21(12):1749–1757.
11. Jacobson SG, et al. (2012) Gene therapy for leber congenital amaurosis caused by *RPE65* mutations: Safety and efficacy in 15 children and adults followed up to 3 years. *Arch Ophthalmol* 130(1):9–24.
12. Chen Y, Moiseyev G, Takahashi Y, Ma JX (2006) *RPE65* gene delivery restores isomerohydrolase activity and prevents early cone loss in *Rpe65-/-* mice. *Invest Ophthalmol Vis Sci* 47(3):1177–1184.
13. Bemelmans AP, et al. (2006) Lentiviral gene transfer of *RPE65* rescues survival and function of cones in a mouse model of Leber congenital amaurosis. *PLoS Med* 3(10): e347.
14. Narfström K, et al. (2008) Morphological aspects related to long-term functional improvement of the retina in the 4 years following rAAV-mediated gene transfer in the RPE65 null mutation dog. *Adv Exp Med Biol* 613:139–146.
15. Kostic C, et al. (2011) Gene therapy regenerates protein expression in cone photoreceptors in *Rpe65*(R91W/R91W) mice. *PLoS One* 6(2):e16588.
16. Li X, et al. (2011) Gene therapy rescues cone structure and function in the 3-month-old rd12 mouse: A model for midcourse *RPE65* leber congenital amaurosis. *Invest Ophthalmol Vis Sci* 52(1):7–15.
17. Mowat FM, et al. (2012) *RPE65* gene therapy slows cone loss in *Rpe65*-deficient dogs. *Gene Ther*, 10.1038/gt.2012.63.
18. Zheng Q, et al. (2012) Differential proteomics and functional research following gene therapy in a mouse model of Leber congenital amaurosis. *PLoS One* 7(8):e44855.
19. Porto FB, et al. (2002) Prenatal human ocular degeneration occurs in Leber's congenital amaurosis (LCA2). *J Gene Med* 4(4):390–396.
20. Jacobson SG, et al. (2008) Photoreceptor layer topography in children with leber congenital amaurosis caused by *RPE65* mutations. *Invest Ophthalmol Vis Sci* 49(10): 4573–4577.
21. Caruso RC, et al. (2010) Retinal disease in Rpe65-deficient mice: Comparison to human leber congenital amaurosis due to *RPE65* mutations. *Invest Ophthalmol Vis Sci* 51(10): 5304–5313.
22. Jacobson SG, et al. (2007) Human cone photoreceptor dependence on RPE65 isomerase. *Proc Natl Acad Sci USA* 104(38):15123–15128.
23. Lorenz B, et al. (2008) A comprehensive clinical and biochemical functional study of a novel *RPE65* hypomorphic mutation. *Invest Ophthalmol Vis Sci* 49(12):5235–5242.
24. Maeda T, et al. (2009) Loss of cone photoreceptors caused by chromophore depletion is partially prevented by the artificial chromophore pro-drug, 9-cis-retinyl acetate. *Hum Mol Genet* 18(12):2277–2287.
25. Cideciyan AV, et al. (2009) ABCA4 disease progression and a proposed strategy for gene therapy. *Hum Mol Genet* 18(5):931–941.
26. Jacobson SG, et al. (2011) Retinal disease course in Usher syndrome 1B due to *MYO7A* mutations. *Invest Ophthalmol Vis Sci* 52(11):7924–7936.
27. Jacobson SG, et al. (2009) Defining the residual vision in leber congenital amaurosis caused by *RPE65* mutations. *Invest Ophthalmol Vis Sci* 50(5):2368–2375.
28. Narfström K, Wrigstad A, Nilsson SE (1989) The Briard dog: A new animal model of congenital stationary night blindness. *Br J Ophthalmol* 73(9):750–756.
29. Wrigstad A, Nilsson SE, Narfström K (1992) Ultrastructural changes of the retina and the retinal pigment epithelium in Briard dogs with hereditary congenital night blindness and partial day blindness. *Exp Eye Res* 55(6):805–818.
30. Wrigstad A, Narfström K, Nilsson SE (1994) Slowly progressive changes of the retina and retinal pigment epithelium in Briard dogs with hereditary retinal dystrophy. A morphological study. *Doc Ophthalmol* 87(4):337–354.
31. Veske A, Nilsson SE, Narfström K, Gal A (1999) Retinal dystrophy of Swedish briard/briard-beagle dogs is due to a 4-bp deletion in *RPE65*. *Genomics* 57(1):57–61.
32. Hernández M, Pearce-Kelling SE, Rodriguez FD, Aguirre GD, Vecino E (2010) Altered expression of retinal molecular markers in the canine RPE65 model of Leber congenital amaurosis. *Invest Ophthalmol Vis Sci* 51(12):6793–6802.
33. Wright AF, et al. (2004) Lifespan and mitochondrial control of neurodegeneration. *Nat Genet* 36(11):1153–1158.
34. Acland GM, et al. (2001) Gene therapy restores vision in a canine model of childhood blindness. *Nat Genet* 28(1):92–95.
35. Acland GM, et al. (2005) Long-term restoration of rod and cone vision by single dose rAAV-mediated gene transfer to the retina in a canine model of childhood blindness. *Mol Ther* 12(6):1072–1082.
36. Cideciyan AV, et al. (2009) Human *RPE65* gene therapy for Leber congenital amaurosis: Persistence of early visual improvements and safety at 1 year. *Hum Gene Ther* 20(9):999–1004.
37. Holmes C, et al. (2008) Long-term effects of Abeta42 immunisation in Alzheimer's disease: Follow-up of a randomised, placebo-controlled phase I trial. *Lancet* 372(9634): 216–223.
38. Wilkinson D, et al. (2012) Memantine and brain atrophy in Alzheimer's disease: A 1-year randomized controlled trial. *J Alzheimers Dis* 29(2):459–469.
39. Clarke G, et al. (2000) A one-hit model of cell death in inherited neuronal degenerations. *Nature* 406(6792):195–199.
40. Herrera W, et al. (2008) Retinal disease in Usher syndrome III caused by mutations in the *clarin*-1 gene. *Invest Ophthalmol Vis Sci* 49(6):2651–2660.

41. Stone EM, et al. (2011) Autosomal recessive retinitis pigmentosa caused by mutations in the *MAK* gene. *Invest Ophthalmol Vis Sci* 52(13):9665–9673.
42. Lai CM, et al. (2004) Recombinant adeno-associated virus type 2-mediated gene delivery into the *Rpe65-/-* knockout mouse eye results in limited rescue. *Genet Vaccines Ther* 2(1):3.
43. Van Hooser JP, et al. (2000) Rapid restoration of visual pigment and function with oral retinoid in a mouse model of childhood blindness. *Proc Natl Acad Sci USA* 97(15):8623–8628.
44. Lorenz B, et al. (2004) Lack of fundus autofluorescence to 488 nanometers from childhood on in patients with early-onset severe retinal dystrophy associated with mutations in *RPE65*. *Ophthalmology* 111(8):1585–1594.
45. Pasadhika S, et al. (2010) Differential macular morphology in patients with *RPE65-*, *CEP290-*, *GUCY2D-*, and *AIPL1*-related Leber congenital amaurosis. *Invest Ophthalmol Vis Sci* 51(5):2608–2614.
46. Narfström K, et al. (2003) Functional and structural recovery of the retina after gene therapy in the RPE65 null mutation dog. *Invest Ophthalmol Vis Sci* 44(4):1663–1672.
47. Dejneka NS, et al. (2004) In utero gene therapy rescues vision in a murine model of congenital blindness. *Mol Ther* 9(2):182–188.
48. Jacobson SG, et al. (2006) Safety of recombinant adeno-associated virus type *2-RPE65* vector delivered by ocular subretinal injection. *Mol Ther* 13(6):1074–1084.
49. Pang JJ, et al. (2006) Gene therapy restores vision-dependent behavior as well as retinal structure and function in a mouse model of *RPE65* Leber congenital amaurosis. *Mol Ther* 13(3):565–572.
50. Aguirre GK, et al. (2007) Canine and human visual cortex intact and responsive despite early retinal blindness from *RPE65* mutation. *PLoS Med* 4(6):e230.
51. Le Meur G, et al. (2007) Restoration of vision in RPE65-deficient Briard dogs using an AAV serotype 4 vector that specifically targets the retinal pigmented epithelium. *Gene Ther* 14(4):292–303.
52. Annear MJ, et al. (2011) Gene therapy in the second eye of RPE65-deficient dogs improves retinal function. *Gene Ther* 18(1):53–61.
53. Woodruff ML, et al. (2003) Spontaneous activity of opsin apoprotein is a cause of Leber congenital amaurosis. *Nat Genet* 35(2):158–164.
54. Cottet S, Schorderet DF (2008) Triggering of Bcl-2-related pathway is associated with apoptosis of photoreceptors in *Rpe65-/-* mouse model of Leber's congenital amaurosis. *Apoptosis* 13(3):329–342.
55. Hamann S, Schorderet DF, Cottet S (2009) Bax-induced apoptosis in Leber's congenital amaurosis: A dual role in rod and cone degeneration. *PLoS One* 4(8):e6616.
56. Métrailler S, Schorderet DF, Cottet S (2012) Early apoptosis of rod photoreceptors in *Rpe65(-/-)* mice is associated with the upregulated expression of lysosomal-mediated autophagic genes. *Exp Eye Res* 96(1):70–81.
57. Kaylor JJ, et al. (2013) Identification of DES1 as a vitamin A isomerase in Müller glial cells of the retina. *Nat Chem Biol* 9(1):30–36.
58. Cottet S, et al. (2006) Biological characterization of gene response in *Rpe65-/-* mouse model of Leber's congenital amaurosis during progression of the disease. *FASEB J* 20(12):2036–2049.
59. Nusinowitz S, et al. (2006) Cortical visual function in the *rd12* mouse model of Leber Congenital Amarousis (LCA) after gene replacement therapy to restore retinal function. *Vision Res* 46(22):3926–3934.
60. Tan MH, et al. (2009) Gene therapy for retinitis pigmentosa and Leber congenital amaurosis caused by defects in *AIPL1*: Effective rescue of mouse models of partial and complete Aipl1 deficiency using AAV2/2 and AAV2/8 vectors. *Hum Mol Genet* 18(12): 2099–2114.
61. Pawlyk BS, et al. (2010) Replacement gene therapy with a human *RPGRIP1* sequence slows photoreceptor degeneration in a murine model of Leber congenital amaurosis. *Hum Gene Ther* 21(8):993–1004.
62. Pang JJ, et al. (2011) Long-term retinal function and structure rescue using capsid mutant AAV8 vector in the *rd10* mouse, a model of recessive retinitis pigmentosa. *Mol Ther* 19(2):234–242.
63. Simons DL, Boye SL, Hauswirth WW, Wu SM (2011) Gene therapy prevents photoreceptor death and preserves retinal function in a Bardet-Biedl syndrome mouse model. *Proc Natl Acad Sci USA* 108(15):6276–6281.
64. Koch S, et al. (2012) Gene therapy restores vision and delays degeneration in the CNGB1/mouse model of retinitis pigmentosa. *Hum Mol Genet* 21(20):4486–4496.
65. Beltran WA, et al. (2012) Gene therapy rescues photoreceptor blindness in dogs and paves the way for treating human X-linked retinitis pigmentosa. *Proc Natl Acad Sci USA* 109(6):2132–2137.
66. Gorbatyuk MS, et al. (2010) Restoration of visual function in P23H rhodopsin transgenic rats by gene delivery of BiP/Grp78. *Proc Natl Acad Sci USA* 107(13):5961–5966.
67. Dalkara D, et al. (2011) AAV mediated GDNF secretion from retinal glia slows down retinal degeneration in a rat model of retinitis pigmentosa. *Mol Ther* 19(9):1602–1608.
68. Ohnaka M, et al. (2012) Long-term expression of glial cell line-derived neurotrophic factor slows, but does not stop retinal degeneration in a model of retinitis pigmentosa. *J Neurochem* 122(5):1047–1053.
69. Trifunović D, et al. (2012) Neuroprotective strategies for the treatment of inherited photoreceptor degeneration. *Curr Mol Med* 12(5):598–612.
70. Komáromy AM, et al. (2010) Gene therapy rescues cone function in congenital achromatopsia. *Hum Mol Genet* 19(13):2581–2593.

Supporting Information

Cideciyan et al. 10.1073/pnas.1218933110

SI Materials and Methods

Human Subjects. ***Retinal cross-sectional imaging and analysis.*** Optical coherence tomography (OCT) scans were obtained with a spectral domain (SD) system (RTVue-100; Optovue). The Line or HD-Line protocols were used to obtain 4.5- or 9-mm-long overlapping scans along vertical meridian crossing the fovea and extending up to 9-mm eccentricity (1, 2). Postacquisition processing of data was performed with custom programs (MatLab 7.5; MathWorks). OCT scans were aligned by the major retinal pigment epithelium (RPE) reflection in each longitudinal reflectivity profile (LRP), registered, merged, and resampled at 512 LRPs per 4.5 mm. Outer photoreceptor nuclear layer (ONL) was segmented manually using a combination of intensity and local slope information of LRPs (2, 3). Specifically, the hyporeflective layer corresponding to the ONL (and the Henle fiber layer) was detected by placing the boundaries at the minimum LRP slope immediately distal (sclerad) to the hyperreflective outer plexiform layer (OPL) and maximum LRP slope proximal (vitread) to the hyperreflective outer limiting membrane (OLM) layer. The ONL was usually first defined in centrally retained regions and extended laterally to more peripheral regions with thinner ONL. Some data from the earliest visit in a subset of patients were acquired on a time-domain system (OCT3; Carl Zeiss Meditec) and analyzed as previously described (4–6).

Because normal ONL thickness changes with eccentricity, a parameter named ONL fraction was derived by dividing ONL thickness measured at each location by the mean normal ONL thickness at the corresponding retinal location (7). ONL fraction values were averaged across 1.2-mm spans between 1.2- and 8.4-mm superior retina and 1.2- and 6-mm inferior retina to reduce noise. A model of disease progression consisting of a delayed exponential function was hypothesized to underlie the change of ONL fraction with age (2, 8). Serial data were obtained in patients in yearly (or longer) intervals, and the rates of exponential decay associated with each pair of sequential data were calculated. The median value of all of the progression rates was assumed to estimate, to a first approximation, the underlying invariant progression rate. Next, the onset of the photoreceptor degeneration was estimated by fitting (least squares on log-linear coordinates) the invariant rate to all data from each individual retinal location and calculating the age at which the function intercepts the unity ONL fraction. The overall variation expected along the natural history of photoreceptor degeneration across all untreated control eyes and all retinal locations was estimated as the 2 SD of the residuals between the data replotted as a function of time after the onset of degeneration and the underlying natural history model (Fig. 1*F*). Serial data from study eyes (both treated and untreated retinal locations) of *RPE65*-LCA were similarly processed to derive ONL fraction. Next, data from each retinal location were horizontally shifted to match the baseline values to the natural history of progression, and the posttreatment values were compared with the expected natural history of degeneration (Fig. 2*B*).

Psychophysical studies. Visual sensitivity of patients was determined with a modified computerized perimeter (Humphrey Field Analyzer; Zeiss) as published (7, 9). The achromatic (white) stimulus was 1.7° in diameter and 200 ms in duration (maximum luminance = 3,180 cd.m^{-2}), and it was presented after patients' eyes were adapted to darkness for an extended (3–8 h) period (7). Tested loci were along the vertical meridian crossing fixation. In all patients, testing was performed in study and control eyes at baseline and posttreatment time points. In a subset of patients, there was additional data available ranging up to 4.5 y before treatment, providing serial measurements for up to 6.7 y. Retinal loci were sampled at 0.6-mm intervals up to 9-mm eccentricity from the fixation. Loci were tested using a red fixation target with a variable intensity that was adjusted to be visible for each subject.

The dynamic range of the native instrument (normally 5 $\log_{10}$ units) was shifted with the use of neutral density filters (up to 3 $\log_{10}$ units) to circumvent ceiling effects that would be otherwise expected in normal subjects and treated regions of some of the patients. In treated eyes, multiple tests were performed with overlapping dynamic ranges; floor or ceiling values were discarded, and best sensitivities were used.

Dogs. ***Retinal cross-sectional imaging and analysis.*** *En face* and retinal cross-sectional imaging was performed with the dogs under general anesthesia (10, 11). Overlapping *en face* images of reflectivity with near-infrared (NIR) illumination (820 nm) were obtained (Spectralis) with 30°- and 55°-diameter lenses to delineate fundus features, such as optic nerve, retinal blood vessels, boundaries of injection blebs, retinotomy sites, and other local changes. Custom programs (MatLab 7.5; MathWorks) were used to digitally stitch individual photos into a retina-wide panorama. In a subset of eyes, short-wavelength (488 nm) illumination was used to delineate the boundary of the tapetum and pigmented RPE. SD-OCT was performed with linear and raster scans (RTVue-100 by Optovue or Spectralis HRA+OCT). Linear scans were placed across regions or features of interest, such as bleb boundaries, to obtain highly resolved local retinal structure. The bulk of the cross-sectional retinal information was obtained from overlapping raster scans (6 × 6 mm, 101 lines of 513 LRPs each, no averaging; Optovue; 9 × 6 mm, 49 lines of 1,536 LRPs each, averaging 8–10; Spectralis) covering large regions of the retina extending ~24 × 24 mm^2.

Postacquisition processing of OCT data was performed with custom programs (MatLab 7.5; MathWorks). For retina-wide topographic analysis, integrated backscatter intensity (OCT projection image) of each raster scan was used to locate its precise location and orientation relative to retinal features visible on the retina-wide mosaic formed by NIR reflectance images. Individual LRPs forming all registered raster scans were allotted to regularly spaced bins (1° × 1°) in a rectangular coordinate system centered at the optic nerve; LRPs in each bin were aligned and averaged. Intraretinal peaks and boundaries corresponding to histologically definable layers were segmented semiautomatically with manual override using both intensity and slope information of backscatter signal along each LRP. Specifically, the retina–vitreous interface, OPL, OLM, signal peak near the inner/outer segment junction, and RPE were defined. In the superior retina of the dog, backscatter from the tapetum forms the highest intensity peak, and RPE and inner/outer segment peaks are located vitreal to the tapetal peak. ONL thickness was defined from the sclerad transition of the OPL to the OLM, and ONL thickness topography was calculated. For all topographic results, locations of blood vessels, optic nerve head, and bleb boundaries were overlaid for reference.

Normal ONL maps were registered by the locus of the optic nerve head and rotated to bring the superior central vessels in congruence. A map of mean normal ONL thickness was derived. *RPE65*-mutant dog ONL maps similarly were registered to the normal map, and an ONL fraction was derived by dividing each thickness by the corresponding mean normal value. This derived ONL fraction map was sampled at five locations: two loci were in

the superior retina, two loci were in the inferior retina, and one locus was in the central nasal retina near the visual streak (Fig. 3 *A*–*C*). Natural history of photoreceptor degeneration was estimated by plotting ONL fraction values at these loci against age.

Electroretinography. Dogs were dark-adapted overnight, premedicated, and anesthetized as described (12–15). Pupils were dilated. Pulse rate, oxygen saturation, and temperature were monitored. Full-field electroretinograms (ERGs) were recorded with Burian–Allen (Hansen) contact lens electrodes and one of two different computer-based systems with similar flash stimuli. Dogs 23–27 (D23–D27) were tested with the EPIC-XL (LKC Technologies) equipment previously described (15). D16, D17, D19, and D22 were tested with an Espion (Diagnosys LLC) system. White flashes (0.4–1.2 log scot-cd.s.m^{-2}) were presented under dark-adapted conditions or flickered at 29 Hz on a rod-desensitizing background (0.8 log cd.m^{-2}). In some case, high-energy flashes were used to evoke photoresponses.

Morphological evaluation. Assessment of photoreceptor structure was made in 6- to 7-μm-thick retinal sections stained with H&E from eyes that were fixed in Bouin or Excalibur solution as previously described (16, 17). Using the *en face* retinal images and ONL topography maps as guides, eyes were trimmed to section through the treated and untreated regions. To correlate the degree of structural preservation with RPE65 expression, immunolabeling of adjacent sections was done with and without antigen retrieval using a polyclonal anti-RPE65 antibody (RPE65 PETLET; a gift from T. M. Redmond, Laboratory of Retinal Cell and Molecular Biology, National Eye Institute, National Institutes of Health, Bethesda) combined, when appropriate, with monoclonal antirhodopsin antibody (MAB5316; Millipore) using methods previously described (17). As control, we used retinal sections processed in the same manner from dogs that were WT or homozygous mutants at the RPE65 locus.

1. Cideciyan AV, et al. (2011) Cone photoreceptors are the main targets for gene therapy of NPHP5 (IQCB1) or NPHP6 (CEP290) blindness: Generation of an all-cone Nphp6 hypomorph mouse that mimics the human retinal ciliopathy. *Hum Mol Genet* 20(7):1411–1423.
2. Jacobson SG, et al. (2011) Retinal disease course in Usher syndrome 1B due to MYO7A mutations. *Invest Ophthalmol Vis Sci* 52(11):7924–7936.
3. Jacobson SG, et al. (2008) Photoreceptor layer topography in children with leber congenital amaurosis caused by RPE65 mutations. *Invest Ophthalmol Vis Sci* 49(10):4573–4577.
4. Huang Y, et al. (1998) Relation of optical coherence tomography to microanatomy in normal and rd chickens. *Invest Ophthalmol Vis Sci* 39(12):2405–2416.
5. Jacobson SG, et al. (2005) Identifying photoreceptors in blind eyes caused by *RPE65* mutations: Prerequisite for human gene therapy success. *Proc Natl Acad Sci USA* 102(17):6177–6182.
6. Jacobson SG, et al. (2007) Human cone photoreceptor dependence on RPE65 isomerase. *Proc Natl Acad Sci USA* 104(38):15123–15128.
7. Cideciyan AV, et al. (2008) Human gene therapy for RPE65 isomerase deficiency activates the retinoid cycle of vision but with slow rod kinetics. *Proc Natl Acad Sci USA* 105(39):15112–15117.
8. Cideciyan AV, et al. (2009) ABCA4 disease progression and a proposed strategy for gene therapy. *Hum Mol Genet* 18(5):931–941.
9. Jacobson SG, et al. (1986) Automated light- and dark-adapted perimetry for evaluating retinitis pigmentosa. *Ophthalmology* 93(12):1604–1611.
10. Cideciyan AV, et al. (2005) In vivo dynamics of retinal injury and repair in the rhodopsin mutant dog model of human retinitis pigmentosa. *Proc Natl Acad Sci USA* 102(14):5233–5238.
11. Beltran WA, et al. (2012) Gene therapy rescues photoreceptor blindness in dogs and paves the way for treating human X-linked retinitis pigmentosa. *Proc Natl Acad Sci USA* 109(6):2132–2137.
12. Acland GM, Aguirre GD (1987) Retinal degenerations in the dog: IV. Early retinal degeneration (erd) in Norwegian elkhounds. *Exp Eye Res* 44(4):491–521.
13. Aguirre GD, Acland GM (1988) Variation in retinal degeneration phenotype inherited at the prcd locus. *Exp Eye Res* 46(5):663–687.
14. Acland GM, et al. (2001) Gene therapy restores vision in a canine model of childhood blindness. *Nat Genet* 28(1):92–95.
15. Acland GM, et al. (2005) Long-term restoration of rod and cone vision by single dose rAAV-mediated gene transfer to the retina in a canine model of childhood blindness. *Mol Ther* 12(6):1072–1082.
16. Jacobson SG, et al. (2006) Safety of recombinant adeno-associated virus type 2-RPE65 vector delivered by ocular subretinal injection. *Mol Ther* 13(6):1074–1084.
17. Kuznetsova TS, et al. (2012) Exclusion of RPGRIP1 ins44 from primary causal association with early-onset cone-rod dystrophy in dogs. *Invest Ophthalmol Vis Sci* 53(9):5486–5501.

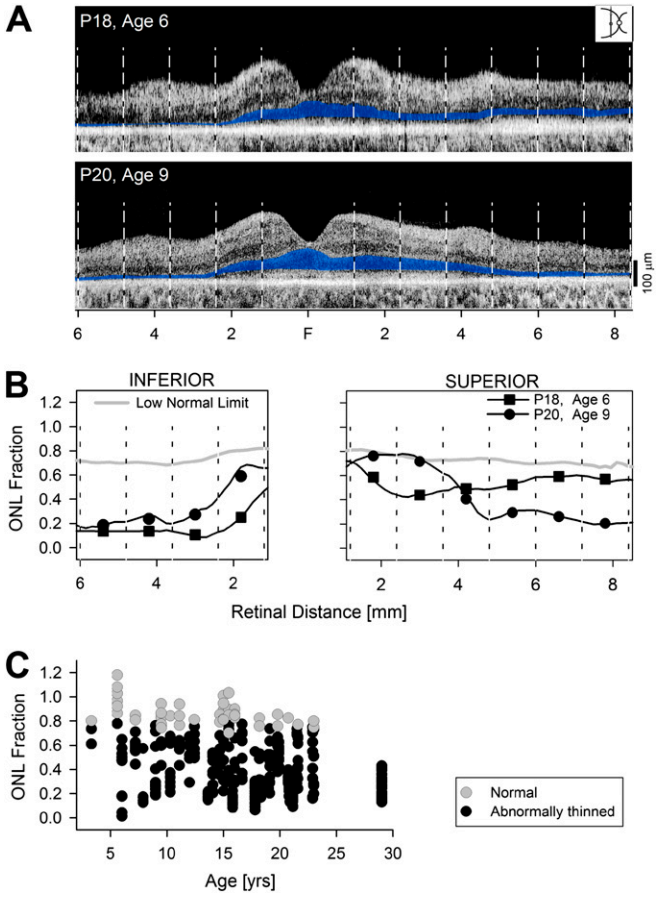

Fig. S1. ONL thickness in patients with *RPE65*-LCA at different ages. (*A*) Cross-sectional retinal images along the vertical meridian crossing the fovea (schematic in *Inset*) in two young patients, patient 18 (P18) and P20, at ages 6 and 9 y, respectively. ONL thickness is colored blue on images. Superior retina is to the right. Vertical dashed lines delimit the 10 retinal regions analyzed in each eye. (*B*) ONL fraction (of mean normal value) of the two patients shown in *A* plotted as function of eccentricity. ONL fraction of unity represents the mean normal at each location, and lower limit (mean − 2 SD) of normal is shown with the gray line. ONL fraction is abnormally thin at all locations in both patients. (*C*) ONL fraction measured along the vertical meridian in patients with *RPE65*-LCA and plotted as a function of age. In *B* and *C*, black symbols represent abnormally thinned loci, and gray symbols represent loci with normal thickness.

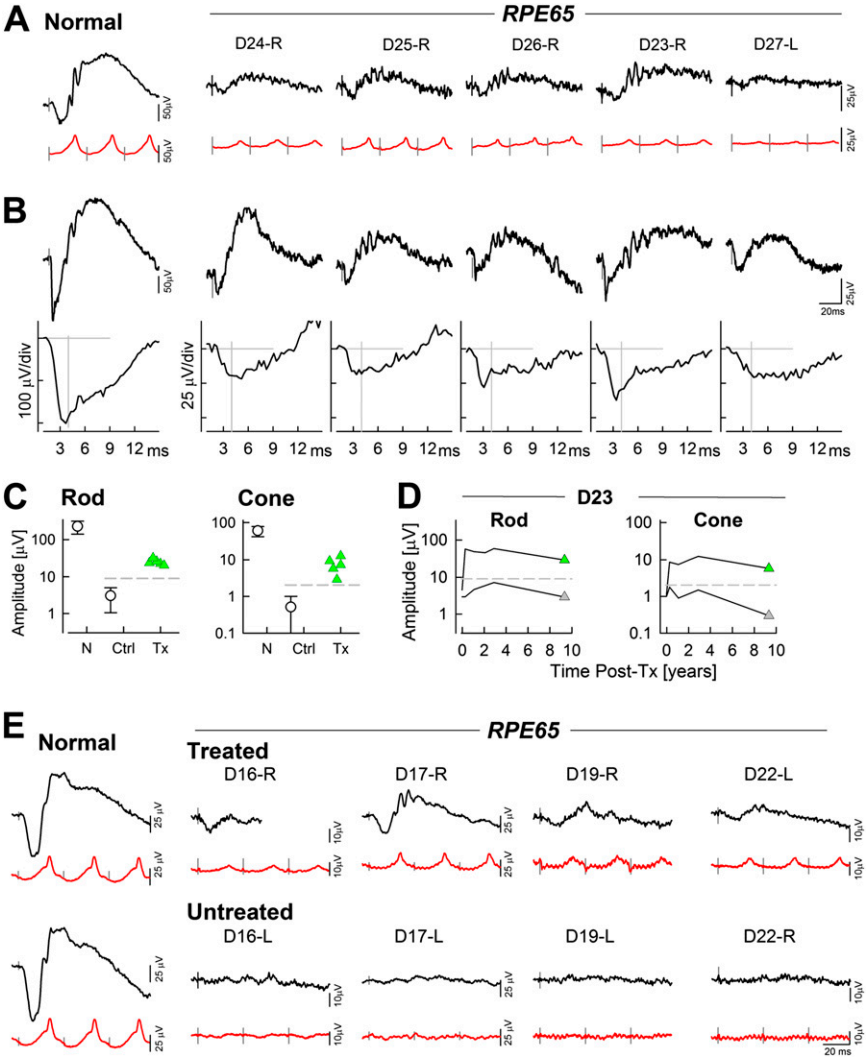

Fig. S2. Restoration of rod and cone retinal function after a single subretinal gene therapy treatment in *RPE65*-mutant dogs treated early and evaluated up to a decade later (*A*–*D*) and treated late and evaluated 1 mo after the treatment (*E*) compared with normal. (*A*) ERGs evoked by standard white flashes presented under dark-adapted (DA) (black traces) or light-adapted (LA) (red traces) conditions. Black vertical lines show the timing of the flashes. (*B*) ERG photoresponses evoked by white flashes of high energy under dark-adapted conditions; same data are shown on slow (*Upper*) and fast (*Lower*) time scales to allow interpretation of late and early components, respectively. Gray lines show the baseline and the 4-ms time point where rod photoreceptor responses were measured. (*C*) Comparison of rod and cone function in the treated *RPE65*-mutant dogs (Tx; green triangles) compared with previously published (15) normal (N) and untreated control (Ctrl) eyes. Rod function shown refers to the DA ERG photoresponse amplitude at 4 ms, and cone function refers to the peak amplitude of the LA 29-Hz waveform. Horizontal dashed lines represent the upper limit (mean + 3 SD) of the respective measurement in the group of control eyes. (*D*) Durability of the rod and cone ERG amplitudes in D23 treated a decade earlier. Subretinally treated right eye is shown with green symbols, and the intravitreally treated left eye is shown with gray symbols. Lines show previously published data extending to age of 3 y (15). Slight reduction of the ERG amplitudes between ages 3 and 10 y is expected from aging effects (12, 13). (*E*) Bilateral ERGs recorded with similar methods and stimuli as shown in *A* in a normal dog and four unilaterally treated *RPE65*-mutant dogs. Treatments were applied at late ages ranging from 4.9 to 6.6 y. ERG recordings performed 1 mo later show definite treatment effects in the eyes with gene therapy.

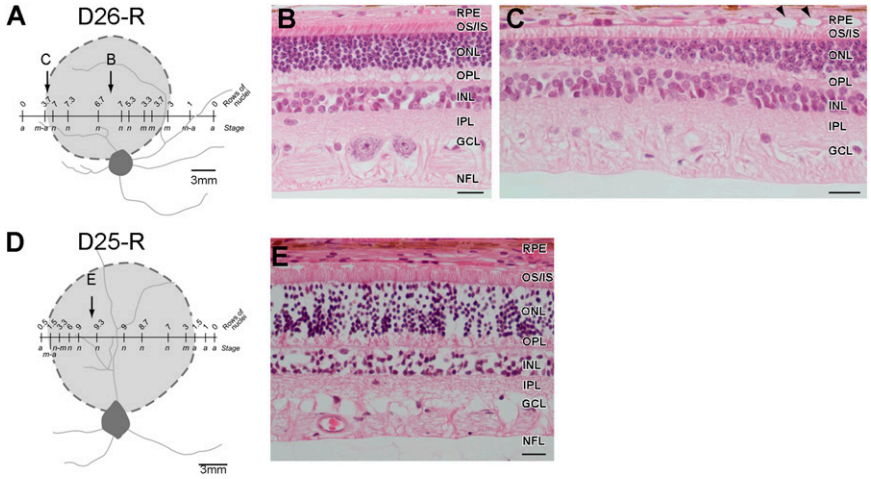

Fig. S3. Gene augmentation therapy at 1.9 y in right eyes of D26 and D25 rescues photoreceptors in the canine LCA. (*A* and *D*) Schematic representation of the *en face* images showing the treatment areas when imaged at 6.7 y of age (dashed lines), on which is superimposed the ONL counts (mean of three values in area sampled) and disease staging (*a*, advanced atrophy with gliosis and loss of retinal layer organization; *m*, moderate photoreceptor loss with 1/3 to 1/2 of ONL remaining; *n*, normal) assessed at 6.9 (D26) and 8.2 (D25) y of age. (*B*, *C*, and *E*) Representative photomicrographs taken from areas identified in *A* and *D*. In the treatment area, there is normal retinal preservation (*B* and *E*). At the edge of the treatment border (*C*), the photoreceptor layer becomes attenuated. GCL, ganglion cell layer; INL, inner nuclear layer; NFL, nerve fiber layer; OS/IS, outer and inner segment layer. (Calibration marker: 20 μm.)

Table S1. Untreated control eyes of *RPE65*-LCA patients

			Retinal structure and visual function	
Patient*	Eye	Mutation	Age at first visit (y)	Follow-up (y)
P1	R	E417Q/E417Q	21	5.5
P2	L	R44Q/R91W	19	6.7
P3	L	Y368H/Y368H	19, 20[†]	6.3, 4.9[†]
P4	L	G40S/H182Y	29	4.2
P5	R	R97del20bp/R97del20bp	17	6.0
P6	R	L341S/L341S	20	4.8
P7	R	IVS1+1G > T/IVS1+1G > T	15	3.4
P8	R	V287F/V287F	13	4.9
P9	R	IVS2-2A > T/L341S	10	3.8
P11	L	V353ins1bp/R91W	23	6.6
P12	L	IVS2-2A > T/L341S	12	4.3
P13	R	R91W/R91W	7	5.1
P14	L	IVS1+5G > A/Y239D	16	1.9
P15	L	Y368H/K354ins1bp	18	1.2
P16	R	R91W/R91W	3	—
P17	R, L	A500del5bp/A500del5bp	5, 9[‡]	—
P18	L	R44Q/R44Q	6	—
P19	L	R44Q/R44Q	7	—
P20	R	A500del5bp/A500del5bp	9	—
P21	L	L408P/L408P	12	—
P22	R	R91Q/R91W	14	—
P23	R, L	G40S/R91Q	19	5.8

L, left eye; R, right eye.

*P1–P15 refer to the untreated eyes of patients taking part in the clinical trial of gene augmentation therapy in the contralateral eye [same nomenclature as used in the work by Jacobson et al. (1)]; P16–P23 refer to patients who have not been treated in either eye. P10 was not included, because severe keratconus and nystagmus in the untreated left eye precluded high-quality imaging. P9 and P12, P13 and P16, P17 and P20, and P18 and P19 are sibling pairs.

[†]Visual function was available for a visit earlier than retinal structure.

[‡]Two eyes were scanned at different visits.

1. Jacobson SG, et al. (2012) Gene therapy for leber congenital amaurosis caused by *RPE65* mutations: Safety and efficacy in 15 children and adults followed up to 3 years. *Arch Ophthalmol* 130(1):9–24.

Table S2. Gene therapy-treated study eyes of *RPE65*-LCA patients

Patient*	Eye	Age at treatment (y)	Retinal structure and visual function follow-up (y)
P1	L	24	2.3
P2	R	23	3.2
P4	R	30	3.1
P6	L	22	3.1
P7	L	15	3.1
P8	L	16	2.2
P9	L	11	2.1
P11	R	27	2.0
P13	L	11	1.0
P14	R	17	1.4
P15	R	18	1.2

*Same nomenclature as used in the work by Jacobson et al. (1) for P1–P15 taking part in the clinical trial of gene therapy. P3, P5, P10, and P12 are not included, because they did not have either a treatment region crossing the vertical meridian or a reliable visual improvement corresponding to the vertical meridian analyzed.

1. Jacobson SG, et al. (2012) Gene therapy for leber congenital amaurosis caused by *RPE65* mutations: Safety and efficacy in 15 children and adults followed up to 3 years. *Arch Ophthalmol* 130(1):9–24.

Table S3. Eyes of *RPE65*-mutant and normal dogs and ages (y) when evaluations were performed

Dog	Eye	Tx	OCT	ERG	Histology
Normal					
D1	R	—	0.1	—	—
D2	R	—	0.3	—	—
D3	R, L	—	0.4	—	—
D4	R	—	—	—	0.6
D5	R	—	—	—	0.6
D6	R	—	0.8	—	—
D7	L	—	2.7	—	—
D8	L	—	3.8	—	—
D9*	L	—	7.4	—	—
D10	R	—	—	—	7.8
D11*	R, L	—	8.0	—	—
RPE65-mutant					
Natural history (no Tx)					
D12	R	—	—	—	1.3
D13	R, L	—	—	—	1.4
D14	L	—	—	—	1.4
D15	L	—	—	—	1.4
D16	L	—	4.8	—	—
D17	L	—	4.8	—	—
D18	L	—	5.0	—	—
D19	L	—	5.1	—	—
D20	R, L	—	5.2	—	—
D21	R, L	—	5.2	—	—
D22	R	—	6.4	—	—
D23	L	—†	9.7	9.7	—
Tx at dysfunction stage/evaluation at dysfunction and degeneration stage					
D24	R	1.8	6.6	6.6	8.1
D25	R	1.9	6.7	6.7	8.2
D26	R	1.9	6.7	6.7	6.9
D27	L	2.4	7.2	7.2	7.2
D23	R	0.3	9.7	9.7	11.2
Tx at dysfunction and degeneration stage/evaluation at dysfunction and degeneration stage					
D16	R	4.9	5.9	5.0	—
D17	R	4.9	5.9	5.0	—
D19	R	5.3	6.3	5.4	—
D22	L	6.6	7.9	6.7	—

L, left eye; R, right eye; —, not performed.
*D9 and D11 are heterozygous carriers of the *RPE65* mutation.
†D23 L was injected intravitreally and is considered effectively as untreated (1, 2).

1. Acland GM, et al. (2001) Gene therapy restores vision in a canine model of childhood blindness. *Nat Genet* 28(1):92–95.
2. Acland GM, et al. (2005) Long-term restoration of rod and cone vision by single dose rAAV-mediated gene transfer to the retina in a canine model of childhood blindness. *Mol Ther* 12(6):1072–1082.